Boletín Geológico, 52(2), 2025
https://revistas.sgc.gov.co/index.php/boletingeo

Research article

Magmatic Evolution of the Panales Caldera: Chemo-mineralogical characterization of the El Torito Dome, Mexico

Evolución Magmática de la Caldera Panales: Caracterización Química-Mineralógica del Domo el Torito, México

Luis Enrique **Ortiz-Hernández** [1], José Cruz **Escamilla-Casas**[1]

[1] Área Académica de Ciencias de la Tierra y Materiales, Universidad Autónoma del Estado de Hidalgo, Mineral de la Reforma, Hidalgo, México, C.P. 42184

Abstract

The aim of the present work is to determine the petrogenetic significance of a dacitic dome in central Mexico, and to establish the correlation with the geological evolution of the eastern sector of the Trans Mexican Volcanic Belt, which traverses the southwestern portion of the state of Hidalgo. For such, we carried out field work campaigns, petrography, quantitative chemical analysis of minerals and constitutive glass through SEM and, as a complement, whole rock chemical analysis and of some trace elements. In the field, a 0.5 km2 dacitic dome was identified and interpret-ed as a resurgent central dome associated with the Panales caldera, which is a presumably Miocene-Late Pliocene, 7 km2, caldera.

Petrographic and geochemical characterization of this dome, indicate that the rock is a calc-alkaline, sodic, moderately potassic and slightly peralkaline, amphibole-dacite (A / CNK = 1.1). Geothermometry and geobarometry suggest that this rock was formed at an intermediate deep crust depth, between 14.8 to 17.4 km (4.0 to 4.7 kbars), and under ranging temperatures between ~ 950 to ~ 800 ° C. Based upon the characterization of the studied dome and on the correlation with adjacent volcanic series of the eastern sector of the Trans Mexican Volcanic Belt, arouses the petrogenetic significance of this dome and the conclusive evidence of the omnipresent occurrence of adakitic volcanism along the Transmexican Volcanic Belt.

Keywords: Petrology, geothermometry, geobarometry, adakite, state of Hidalgo, central Mexico, Transmexican Volcanic Belt

Resumen

El objetivo del presente trabajo es determinar el significado petrogenético de un domo de dacita ubicado en el centro de México, y correlacionarlo con la evolución geológica del sector oriental de la Faja Volcánica Transmexicana, misma que atraviesa parte de la porción sudoccidental del estado de Hidalgo. Para ello, se realizaron campañas de trabajo de campo, estudio petrográfico y análisis químico cuantitativo de minerales y vidrio constitutivo de la roca mediante microscopio electrónico de barrido, complementado con el análisis geoquímico de roca total y de algunos elementos traza. En el trabajo de campo se identifica al domo dacítico de 0.5 km2, como domo central resurgente de la caldera Panales, de 7 km2, la cual es probablemente del Mioceno-Plioceno tardío.

Petrográfica y geoquímicamente, el domo es una dacita de anfíbol, calco alcalina, sódica, medianamente potásica y ligeramente peralcalina (A/CNK=1.1). La geotermometría y geobarometrìa indican una profundidad de formación cortical-intermedia, entre los 14.8 y 17.4 km (4.0 a 4.7 kbar), y en un rango de temperatura de ~950 a ~800 °C. Tomando como base la caracterización del domo y correlacionándolo con series volcánicas adyacentes de este sector oriental de la Faja Volcánica Transmexicana, se manifiestan el significado petrogenético del domo estudiado y la evidencia concluyente de la ocurrencia de vulcanismo adakítico, omnipresente a lo largo de la Faja Volcánica Transmexicana

Palabras clave: petrología, geotermometría, geobarometría, adakita, estado de Hidalgo, Faja Volcánica Transmexicana

Citation: Ortiz-Hernández, L., Escamilla; J.C. (2025). Magmatic Evolution of the Panales Caldera: Chemo-mineralogical characterization of the El Torito Dome, Mexico. Boletín Geológico, 52(2).
https://doi.org/10.32685/0120-1425/bol.geol.52.2.2025.764

Manuscript received: November 9, 2025
Updated received: December 12, 2025
Manuscript accepted: December 22,2025

Boletín Geológico: ISSS: printed; 0120-1425, ISSN electronic: 2711-1318

1. INTRODUCTION

The formation of a collapse caldera sometimes occurs after depletion induced by deformation of the overlying rocks lead by magma withdrawal from a shallow chamber. Additionally, magmatic calderas develop from the evacuation and depletion of subsurface magma reservoirs, resulting on circular to elliptical collapsed depressions. The topographic expression of collapse calderas rises from the underlying fault architecture that accommodates the downward movement of the overlying rocks into the depleted magma system (Cole et al., 2005; Lipman, 1997; Acocella, 2007). Experimental analogue models of collapse calderas strongly suggest the generation of ring fault systems (e. g. Sillis-Esquivel, 2011; Geyer & Martí, 2014). Likewise, caldera collapse and post-caldera resurgence promote the formation of distinctive structural features such as ring faults and resurgent domes (Lipman, et al., 2015; Galetto et al., 2017).

In the Mexican territory, volcanic rocks dominate a substantial portion of the bedrock geology, being the Neogene-Quaternary Trans Mexican Volcanic Belt (TMVB) the geologic province that hosts active volcanism and magmatic calderas, among other major volcanic features (Mooser, 1972; Demant 2019, Gómez Tuena et al., 2005; among others). Within the TMVB, previous authors studied diverse caldera complexes: La Primavera (Mahood, 1980), Amealco (Aguirre-Díaz, 1996, 2019; Aguirre-Díaz & Mc Dowell, 2000), Los Azufres (Campos Enríquez & Garduño-Monroy, 1995), Mazahua (Anguita et al., 1991), Los Humeros (Ferriz & Mahood, 1987), and Chiconquiaco (Negendank et al., 1985); Figure 1. On the other hand, rocks in southwest Hidalgo are part of the eastern sector of the TMVB and, among diverse landforms and lithological variations, contain volcanic calderas, e.g. Tulancingo-Acoculco Caldera Complex (López-Hernández et al., 2009), Huichapan (Milán et al., 1993; Aguirre-Díaz et al., 1997); Mezquital (Ortiz Hernández & Hernández-Avelino, 2006), Tolteca (Barrera Guerrero & Ortiz-Hernández, 2007) and Panales (Anguita, 2001; Barrera Guerrero, 2009; Reyes-Moreno et al., 2019); Figure 1 and 2.

Barrera-Guerrero (2009) described the Panales caldera and recently, Ortiz-Hernández & Escamilla Casas (2021) studied a dioritic intrusive body and interpreted it as part of the underlying magmatic chamber. The present study focuses on the Panales Caldera, an underexplored volcanic complex within the eastern TMVB (Figure 2a and 2c), aiming to elucidate its magmatic evolution through detailed chemo-mineralogical analysis of the El Torito Dome (Figure 2c, 2d, and 3).

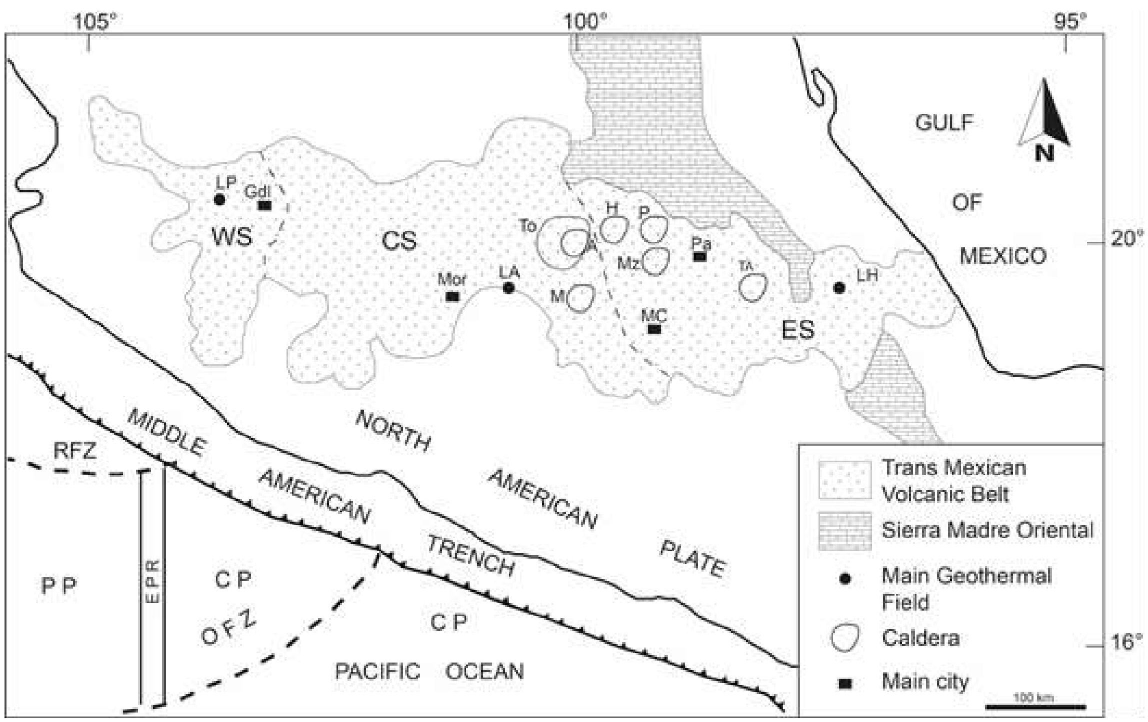

Figure 1. Schematic geologic map showing the main tectonic features: CP, Cocos Plate; EPR, East Pacific Rise; OFZ, Orozco Fracture Zone; PP, Pacific Plate; RFZ, Rivera Fracture Zone. In solid circles, the main geothermal fields: LP, La Primavera; LA, Los Azufres; LH, Los Humeros. Calderas are shown as open round shapes: A, Amealco; H, Huichapan; M, Mazahua; To,Tolteca; Mz, Mezquital; P, Panales, this study; TA, Tulancingo-Acoculco. Trans Mexican Volcanic Belt division: WS, western sector: CS, central sector; ES, eastern sector. For reference, the main cities are shown in solid squares: Gdl, Guadalajara; Mor, Morelia; MC, Mexico City; Pa, Pachuca (Modified from López-Hernández et al., 2009).

Despite the short extension of this dome (0.5 km2 of cropping out rock) its characterization sheds light into the understanding of its petrogenetic significance under the context of the magmatic evolution of the Panales Caldera and of this sector of Hidalgo. This multi-mineral approach provides robust constraints on pre-eruptive magma storage conditions, including temperature, pressure, crucial for assessing the adakitic character of the El Torito dome.

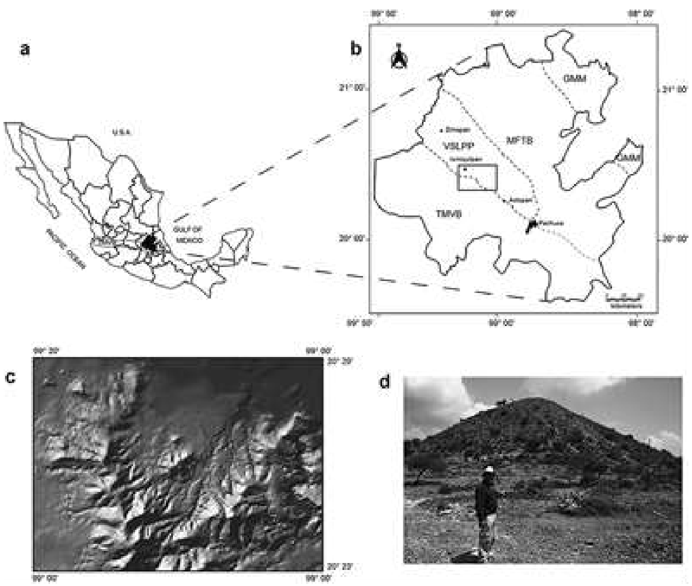

Figure 2. **a** – Location map of the state of Hidalgo in central Mexico. **b** – Geologic provinces of the state of Hidalgo, showing the Panales structure (rectangle) in the limits between the Trans-Mexican Volcanic Belt (TMVB) and Valles-San Luis Platform (VSLPP); MFTB=Mexican Folds and Thrust Belt, GMM=Gulf of Mexico Miogeoclinal. **c** – Satellite image of the Panales structure, El Torito dome at the center. **d** – General view of the El Torito dome.

2. GEOLOGICAL FRAMEWORK

The mid-southern portion of Hidalgo state in central Mexico consists of the relatively young, Miocene-Quaternary, Trans-Mexican Volcanic Belt (TMVB) geologic province (Ferrari et al., 2012; Gómez-Tuena et al., 2005) (Figure1, 2a, and 2b). The TMVB is one of the largest volcanic arcs on the North America Plate, that dissects the Mexican territory by the middle, extending from the Pacific Ocean to the coast of the Gulf of México, along a 1000 km stretch and variable width, between 80-200 km. This significant magmatic province developed, according to modern plate models, as a direct consequence of the subduction of the oceanic Cocos and Rivera plates beneath the North American continental lithosphere, along the Middle America Trench (Weber et al., 2020).

Pasquaré (1987) divided the TMVB in three sectors: (1) the western sector comprising volcanism engulfing the Tepic-Zoacalco rift and Colima graben; (2) the central sector comprising west of Colima and Chapala grabens and limited by the Taxco-San Miguel de Allende Fault system; and (3) the eastern sector engulfing the basins of Toluca, México, Puebla-Tlaxcala and the Cofre de Perote-Pico de Orizaba volcanic range. Later, this domain was extended to the Gulf of Mexico coast by Ferrari et al. (2012).

The TMVB is characterized by a complex tectonic history, with magmatic evolution proceeding through distinct stages, including the Laramide orogeny, an initial stage of TMVB development, Miocene NE-SW extension, and later Pliocene-Quaternary normal faulting controlling the emplacement of various magmatic suites (Gómez-Alvarez et al., 2021).

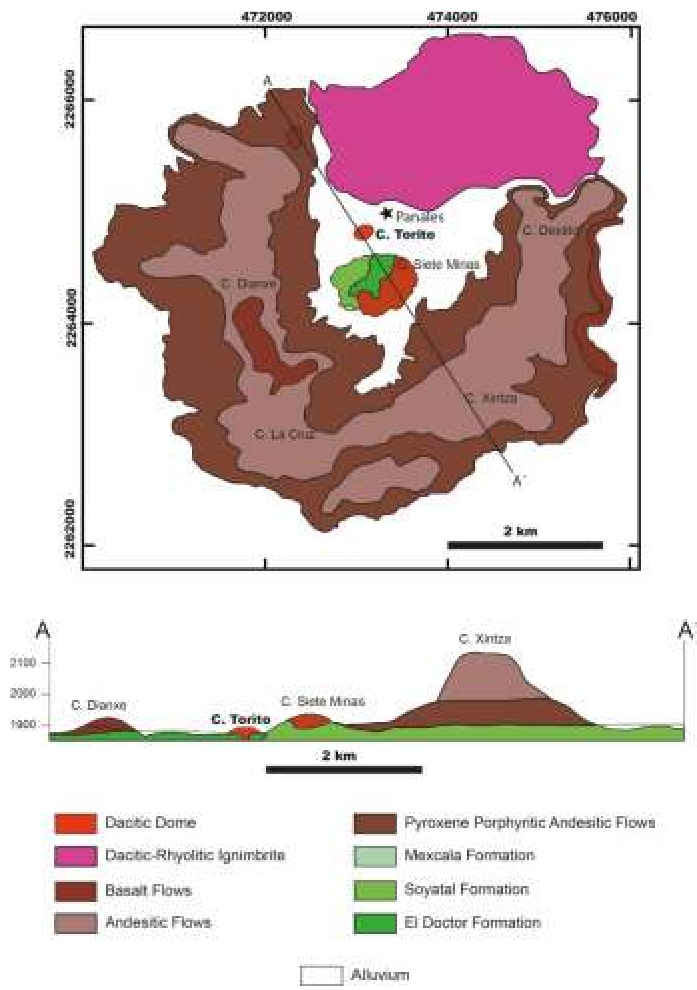

Figure 3. General geological map and cross section of the Panales caldera -named after the village of Panales. To the southwest of Panales, is located El Torito dome (modified from Barrera-Guerrero, 2009).

The volcanic output along the Middle American subduction system, which includes the TMVB, is notably unevenly distributed, reflecting significant variations in the subducting Cocos plate along strike and down dip (Liu & Gao, 2023). This variation in subduction dynamics contributes to the arc's segmented geological structure and diverse magmatic compositions, ranging from basaltic andesites to rhyolites with calc-alkaline affinities (Maldonado-Sánchez & Schaaf, 2005). The complexity of the subduction system, the magmatic diversity, and obliquity with respect to the Middle American Trench has been explained through diverse tectonic models, e.g., mantle plume (OIB-type magmas; Márquez et al., 1999), extensional tectonic setting (Sheth et al., 2000; Sheth et al., 2002; Verma, 2002; Velasco-Tapia and Verma, 2012).

Particularly, in the eastern sector of the TMVB, these dramatic changes in rock composition are attributed to a gradual increase in the angle of subduction by the end of the Miocene (Gomez-Tuena et al., 2003). Moreover, to explain the adakitic signature observed in rocks in the eastern sector of the TMVB, a model that involves the flow of mantle materials through a slab tear has been proposed (Davies & von Blanckenburg, 1995; Guivel et al., 2006; Ribeiro et al., 2016).

The eastern sector of the TMVB involves discrete volcanic fields, with predominance of mono-genetic volcanoes, but in the northeastern sector, calderas, domes, cinerite cones and lavic flows (Castro-García and Córdoba-Méndez, 1994; García-Palomo et al., 2002; García Tovar et al., 2015; Juárez-López 2015; Aparicio-Canales and Contreras-Cruz, 2016; Ramírez-Ramírez, 2016; García- Palomo et al., 2018) are conspicuous.

The study area - 99° 00'-99°20' and 20° 15'- 20°30', geographic coordinates - which comprises the northwestern portion of the Ixmiquilpan geologic chart (Consejo de Recursos Minerales, 1995) is in the transition between the TMVB and the Mesozoic Valles-San Luis carbonate plate (VSLPP, Figure 2a and 2b) and palaeogeographically, belongs to the Ixmiquilpan limestone bank (Segerström, 1961) or Actopan platform (Carrasco, 1971). Throughout the region, there are outcroppings of folded and faulted Cretaceous marine rocks (Albian-Cenomanian El Doctor, Cenomanian-Maastrichtian Mexcala, and Turonian-Coniacian Soyatal formations) partially covered by Tertiary volcanic rocks (andesites and dacites), Eocene-Oligocene detritic fluviolacustrine (El Morro fanglomerate) and Pliocene (Tarango Formation) rocks, Tertiary intrusions and Plio-Quaternary fissure basaltic flows (Consejo de Recursos Minerales, 1995; Barrera-Guerrero, 2009). At present, no basement rocks have been identified in this or in previous works.

In the area of study, a NE-SW trending, horseshoe-shaped, ±7 km2, Miocene-Late Pliocene volcanic caldera was identified by means of satellite imagery (Anguita et al., 2001; Figure 2c, 2d , and 3) and geological mapping at different scales (Consejo de Recursos Minerales, 1995; Barrera-Guerrero, 2009; Reyes-Moreno et al., 2019). This caldera was informally named Panales, after the nearby village. Three volcanic episodes in the evolution of the Panales caldera have been identified: 1. The pre-caldera event, characterized by the extrusion of basaltic and andesitic lavas at the rim of the structure. 2. Caldera formation and collapse, including an ignimbritic explosion. 3. The resurgent event, in which occurred the emplacement of dikes and domes were formed at the center of the structure (Barrera-Guerrero, 2009). Particularly, the morphology of El Torito dome contrasts with the surroundings due to its short extension - a ± 5km2 dome with altitude of ±1900 meters above sea level, with slightly inclined slopes, occurring at the mid portion of the Panales volcanic caldera and interpreted here, as a resurgent dome.

3. METHODS

The studied El Torito dome covers a limited surface area of approximately 0.5 km2 and is characterized by a remarkably homogeneous lithology at both outcrop and hand-sample scales. In the field were not identified compositional layering, textural variations, multiple intrusive or eruptive pulses, nor evidence of magma mingling or significant post-emplacement alteration that would suggest internal geochemical heterogeneity. Therefore, four rock samples were collected. Three samples were studied petrographically (two from the middle and one from the base), the reminding sample was chemically analyzed (from the top of the dome).

The analyzed sample was collected from a fresh, unaltered and representative outcrop, away from structural discontinuities, hydrothermal zones, or chilled margins, ensuring that the obtained whole-rock compositions reflect the primary magmatic signal. The geochemical dataset shows internally consistent major and trace element concentrations, low loss-on-ignition values, and element ratios indicative of a single, chemically coherent magmatic batch.

In volcanic bodies of comparable size and lithological uniformity, previous studies have shown that a single representative whole-rock analysis is sufficient to constrain bulk composition and first-order petrogenetic interpretations. Additional sampling would therefore be analytically redundant and unlikely to provide meaningful constraints on magmatic processes at the scale addressed in this study. Accordingly, the sampling strategy adopted here is considered methodologically sound and appropriate for the objectives of this work.

For such, the whole rock analysis was obtained through X-ray fluorescence, using a Phillips MagixPRO spectrometer being operated by the Servicio Geológico Mexicano (SGM). The rock sample was pulverized at a -200 mesh and analyzed according to rigorous standards, yielding ≧ 95% accuracy in weight percent values. Trace elements were acquired (ppm) by induced coupled mass spectrometry (ICPMS) using a VGElemental instrument, PalmaQuad3 model, also at SGM. Fifteen 30 µm thin sections were prepared by the Servicio Geológico Mexicano, subsequently studied and photographed in the Optical Microscopy Laboratory of the Universidad Autónoma del Estado de Hidalgo, using a Leitz BA310 pol petrographic microscope.

Quantitative analyses of feldspar, amphiboles and volcanic glass were obtained by using natural and synthetic standards at the University Laboratory of Petrology of the Institute of Geophysics, UNAM, in a scanning electron microprobe JEOL JXA-8900R, with WDS and EDS spectrometers, and four crystal-types TAP (5.69~93.0 Å), PETJ (1.93~8.10 Å), LIF (0.889~3.73 Å) and LDE2 (23.2~88.0 Å) allowing an element detection range between beryl and uranium. The applied analytical conditions were 20 kV acceleration voltage, 10 nA beam current, 6 to 10 seconds counting time per group of three elements, and 3µm beam size.

Acquired data were adjusted by depth and ray absorption according to the correction program (ZAF). Structural formulae of plagioclase were calculated based on stoichiometry of 8 atoms of oxygen and 5 cations. For the amphibole, structural formulae were calculated based on anhydrous, 23 oxygens and 13 cations using the AMPH-CLASS computer program (Esawi, 2004). Glass composition in dacite groundmass was determined by electron microprobe, 4 nA beam current and 10 seconds counting time to minimize Na-loss in the chemical analysis. These analyses provide crucial data for understanding the magmatic processes and differentiation pathways that influenced the formation and evolution of the El Torito Dome within the Panales Caldera.

4. RESULTS

4.1 Petrography

Rock samples collected at El Torito dome, present porphyritic texture and microlithic groundmass with euhedral to subhedral phenocrysts of zoned plagioclase and Ca-amphibole with oxidized rims. Phenocrystals are embedded in a microlithic groundmass of plagioclase and k-spar microliths, embedded in acidic glass and scarce anhedral quartz grains. Disseminated opaque minerals are also present (Figure 4). Petrographycally, these rocks are classified as amphibole-dacite.

Plagioclase composition varies between labradorite and andesine (Ab43-67 An28-55 Or0-5), while the composition of k-spar is anorthoclase (Ab55-63 An14-24 Or15-31) (Table 1 and Figure 5a). Both minerals are located between the 700° and 900° isotherms of the triangle of feldspars (Elkins & Grove, 1990).

Amphiboles are calcic $(Ca+Na)_B \geq 1.50$ and $Na_B < 0.50$), with a $Mg/Mg+Fe^{2+}$ ratio between 0.99-1.00 (Table 2), and are tschermakites ($Ca_2Mg_3Fe^{3+}_2Al_2Si_6O_{22}(OH)_2$), (Leake et al., 1997; Figure 5b), with homogeneous silica (43-45%) and high TiO_2 contents (commonly above 2%) with high and variable FeO (10-15%) mainly at the rim of the crystals. Amphiboles are aluminous with slightly variable Al_2O_3 contents, ranging between 10.81-11.89%, depicting a hydrated magma character (Annen et al., 2006).

Figure 4. Photomicrograph (10X, PPL) showing subhedral and anhedral zoned plagioclase crystals and calcic amphibole phenocrystals with oxidizing borders, embedded in a plagioclase and potassium feldspar microlithic groundmass intergrowth with volcanic glass and scarce quartz and opaque minerals (Amp: amphibole; Pl: plagioclase).

Al^{IV} content is greater than Al^{VI}, suggesting that the main substitution is pargasite-hastingsite type in the non-quadrilateral amphibole components, indicating variations of NaM_4, Fe^{3+}, Ti and Al^{IV} in the structural formulae. This can be possibly explained by means of the oxidation during magmatic differentiation, by an increment in fO_2, also supported by the high $Mg/Mg+Fe^{2+}$ ratio and the abundance of opaque minerals in the rock (Luo et al., 2024).

In El Torito dome, amphiboles are significantly more aluminous than corresponding hornblende in volcanic arc rocks, but from the perspective of Ca-Mg-Fe+Mg composition, are like amphiboles in island arc dacitic volcanic rocks. In this rock, amphiboles are Fe-rich, and according to Na_2O vs SiO_2 contents, are classified as amphiboles formed in a supra-subduction context (Coltorti et al., 2007).

Table 1. Chemical composition and structural formula of feldspars[1]

	1	2	3	4	5	6	7	8	9	10	11	12	13	14
SiO_2	58.80	53.10	55.90	55.30	55.00	55.50	55.50	63.10	60.50	58.00	56.70	57.90	62.10	63.20
TiO_2	0.00	0.00	0.00	0.01	0.00	0.00	0.00	0.07	0.00	0.01	0.00	0.01	0.03	0.01
Al_2O_3	25.50	29.00	27.30	27.50	27.70	27.70	27.90	22.90	24.50	26.80	27.30	26.40	24.10	21.40
FeO	0.06	0.37	0.18	0.16	0.16	0.17	0.14	0.23	0.33	0.40	0.34	0.50	0.28	0.36
MgO	0.00	0.02	0.01	0.00	0.01	0.02	0.01	0.00	0.01	0.00	0.00	0.38	0.56	0.72
MnO	0.06	0.05	0.00	0.00	0.00	0.06	0.02	0.06	0.04	0.01	0.03	0.08	0.20	0.01
CaO	7.00	11.10	9.34	9.56	9.86	9.77	9.77	6.31	6.93	8.64	9.60	8.09	5.80	3.34
Na_2O	6.78	4.59	5.90	5.66	5.58	5.60	5.67	7.32	6.65	7.01	6.49	6.94	7.69	7.18
K_2O	0.78	0.32	0.40	0.36	0.40	0.40	0.29	0.87	0.71	0.34	0.36	0.40	0.82	3.69
Total	99.00	98.60	99.00	98.50	98.70	99.20	99.30	101.00	99.70	101.00	101.00	101.00	101.00	99.70
Si	2.66	2.44	2.53	2.53	2.51	2.52	2.51	2.81	2.72	2.56	2.52	2.57	2.73	2.82
Al	1.36	1.57	1.46	1.48	1.49	1.48	1.49	1.20	1.30	1.40	1.43	1.38	1.25	1.13
Fe^{2+}	0.00	0.01	0.10	0.01	0.01	0.01	0.01	0.01	0.10	0.02	0.01	0.02	0.01	0.01
Ca	0.34	0.55	0.46	0.47	0.48	0.48	0.47	0.30	0.34	0.41	0.46	0.39	0.28	0.16
Na	0.59	0.41	0.52	0.50	0.49	0.49	0.50	0.63	0.58	0.60	0.56	0.60	0.66	0.63
K	0.05	0.20	0.02	0.20	0.02	0.02	0.02	0.05	0.04	0.02	0.02	0.02	0.05	0.21
Total	5.00	5.00	5.00	5.00	5.00	5.00	5.00	5.00	5.00	5.00	5.00	5.00	5.00	5.00
Ab	60.40	42.00	52.00	50.60	49.40	49.70	50.40	64.30	60.80	58.40	53.90	59.50	67.30	62.70
An	34.70	56.10	45.60	47.30	48.30	47.90	48.00	30.60	35.00	39.80	44.10	38.30	28.00	16.10
Or	4.60	1.93	2.33	2.12	2.33	2.34	1.70	5.03	4.27	1.86	1.97	2.25	4.72	21.20

[1]Electron microprobe results

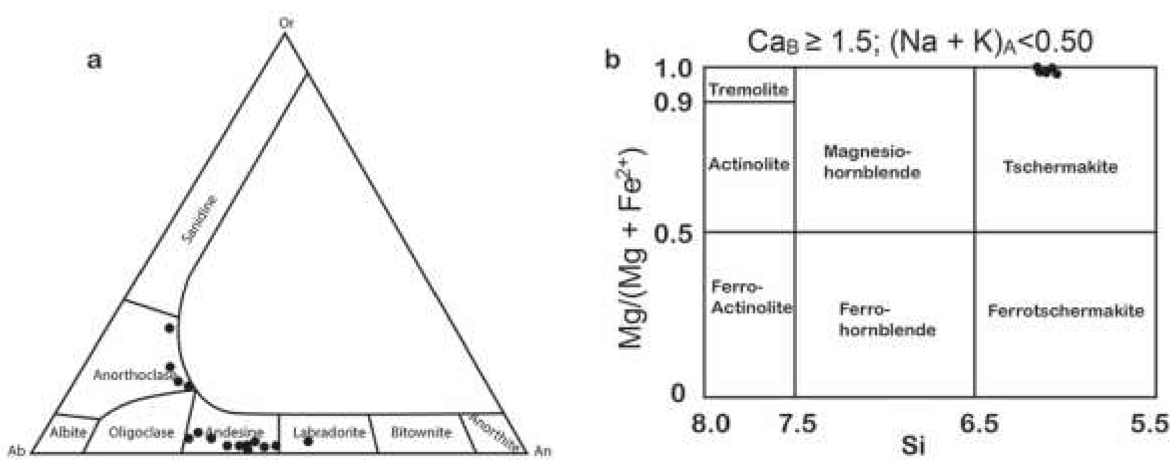

Figure 5. Mineral classification of El Torito dome. a – Triangular feldspar classification, b – Classification of amphiboles according to the nomenclature of Leake et al. (1997)

4.2 Whole-rock Geochemistry

The homogeneous lithology in the El Torito dome allowed us to analyze a single sample. The rock is silica-poor dacite (SiO_2=61.80%), aluminous (Al_2O_3>15%), with low TiO_2 (0.45%) contents. The addition of alkalis (K_2O + Na_2O) in the rock is around 5, with trondhjemitic composition (CaO/Na_2O < 1 = 0.93). It is also ferromagnesian-poor (Fe_2O_3+MgO+MnO+TiO_2=5.26%; Table 3) and has moderate MgO contents (1.33%) #Mg=26 and is slightly peraluminous (ASI = 1.11). The dome is derived from a typical dacitic lava with calc-alkaline affinity, moderately potassic (K_2O=1.72%), and sodic K_2O/Na_2O=0.48 (Figure 6a, b and c). This ratio is close to high silica adakites (HSA=0.47) so is the TiO_2 (<0.9%) value (Martin et al., 2005).

Table 2. Chemical composition and structural formula of calcic amphiboles[1]

	1	2	3	4	5	6	7	8	9	10	11
SiO_2	43.88	44.21	43.94	43.93	43.52	44.59	44.48	44.09	44.18	44.18	44.17
TiO_2	2.13	2.06	2.28	2.27	2.37	2.25	2.26	2.33	2.27	1.72	2.29
Al_2O_3	11.76	11.28	11.42	11.56	11.61	11.20	11.24	11.31	11.67	10.81	11.39
FeO	9.59	9.86	12.15	10.45	10.16	10.36	10.49	10.37	10.32	15.30	9.91
MnO	0.13	0.23	0.21	0.22	0.19	0.16	0.24	0.14	0.15	0.36	0.14
MgO	17.53	18.10	16.19	16.95	16.76	17.69	17.79	17.37	17.01	14.72	17.31
CaO	11.13	11.20	11.52	11.49	11.45	11.46	11.36	11.57	11.38	10.74	11.43
Na_2O	2.24	2.06	2.13	2.28	2.17	2.15	2.22	2.07	2.16	1.91	2.22
K_2O	0.43	0.40	0.47	0.48	0.45	0.43	0.38	0.41	0.45	0.54	0.35
Total	98.82	99.40	100.31	99.63	98.68	100.29	100.46	99.66	99.59	100.28	99.21
Si	6.14	6.15	6.10	6.12	6.12	6.16	6.14	6.13	6.14	6.16	6.16
Al^{iv}	1.86	1.85	1.87	1.88	1.89	1.82	1.83	1.85	1.86	1.78	1.84
Al^{vi}	0.08	0.00	0.00	0.02	0.04	0.00	0.00	0.00	0.06	0.00	0.03
Ti	0.22	0.22	0.24	0.24	0.25	0.23	0.24	0.24	0.24	0.18	0.24
Fe^{3+}	1.12	1.15	1.36	1.22	1.19	1.20	1.21	1.21	1.20	1.73	1.16
$Fe2^{+}$	0.00	0.00	0.05	0.00	0.00	0.00	0.00	0.00	0.00	0.06	0.00
Mn	0.02	0.03	0.03	0.03	0.02	0.02	0.03	0.02	0.02	0.04	0.02
Mg	3.66	3.76	3.35	3.52	3.51	3.64	3.66	3.60	3.53	3.06	3.60
Ca	1.67	1.67	1.71	1.72	1.72	1.70	1.68	1.72	1.70	1.60	1.71
Na	0.61	0.56	0.57	0.62	0.59	0.58	0.59	0.56	0.58	0.52	0.60
K	0.08	0.07	0.08	0.09	0.08	0.08	0.07	0.07	0.08	0.10	0.06
$(Ca+Na)_{(B)}$	1.90	1.85	2.00	1.98	1.98	1.93	1.90	1.95	1.96	2.00	1.96
$Na_{(B)}$	0.24	0.18	0.29	0.27	0.26	0.23	0.22	0.22	0.27	0.40	0.25
$(Na+K)_{(A)}$	0.45	0.45	0.37	0.44	0.41	0.42	0.44	0.41	0.39	0.22	0.42
$Mg/(Mg+Fe^2)$	1.00	1.00	0.99	1.00	1.00	1.00	1.00	1.00	1.00	0.98	1.00
$Fe^3/(Fe^3+Al^{vi})$	0.94	1.00	1.00	0.99	0.97	1.00	1.00	1.00	0.96	1.00	0.97
Total	13.10	13.15	13.00	13.02	13.02	13.08	13.10	13.05	13.04	13.00	13.05
H&Z	5.80	5.40	5.50	5.60	5.80	5.30	5.30	5.40	5.70	5.00	5.50
Holl	6.20	5.70	5.80	5.90	6.10	5.50	5.50	5.70	6.00	5.30	5.80
J&R	4.70	4.40	4.40	4.60	4.70	4.30	4.30	4.40	4.60	4.10	4.50
Sch	6.20	5.80	5.90	6.00	6.10	5.70	5.70	5.80	6.10	5.40	5.90

[1]Electron microprobe results formulae based on anhydrous (23 Oxygens) and 13 cations, using Esawi (2004) computer program. Pressure values were obtained through diverse geobarometers: H&Z=Hammasatron and Zen (1986), Holl=Hollister et al. (1987), J&R=Johnson and Rutherford (1989), Sch=Schmidt (1992).

When comparing previously reported Miocene adakites from this sector of the TMVB – including Apan (APA84; García Palomo et al.,2002), El Ventoso andesitic dome (Ep-14 Aparicio-Canales and Contreras-Cruz, 2016), San Cristobal andesite (SP-12; Martínez González, 2018), and a dacitic flow (PT-1; Ortiz-Hernández and Escamilla-Casas, 2024) – with the El Torito dome, it is observed that the latter is enriched in SiO_2 and TiO_2, while being depleted in MgO and CaO.

Discrimination diagrams (TAS Total Alkalis vs Silica) indicate that the studied rock falls within the subalkaline field (Figure 6a), like other adakitic rocks and a silica-rich adakite reported by Martin et al. (2005). Additionally, the AFM (alkalis, iron, and magnesium) diagram demonstrates its calc-alkaline affinity. The An-Ab-Or normative diagram (Barker, 1979), which is ideal for silica rocks discrimination, shows that this rock falls in the tonalite field (not shown). In contrast, the An-Ab´-Or triangular diagram reveals a sodic character, except for the dacitic flow and the silica-rich adakite (Figure 6c).

Table 3. Whole rock chemical analysis[1]

SiO_2	66.1	Cr	87	Sm	3.93	qz	29.64
TiO_2	0.45	Sc	9	Eu	1.7	pl	49.58
Al_2O_3	15.25	V	39	Gd	3.83	or	10.7
FeO	0.39	Cu	69	Dy	2.24	cor	1.33
Fe_2O_3	3.05	Zr	111	Er	1.15	hyp	6.1
MnO	0.04	Y	14	Yb	0.88	il	0.89
MgO	1.33	Nb	18	Lu	0.13	mt	1.59
CaO	3.32	Th	3	Pr	5.48	ap	0.16
Na_2O	3.57	La	21.99	$(La/Yb)_N$	17.91		
K_2O	1.72	Ce	43.73	Eu/Eu*	0.66		
P_2O_5	0.07	Nd	19.81	Ce/Ce*	0.55		
PXC	2.68						
Total	97.97						

[1] Values in % wt, trace elements in ppm, CIPW norm is also shown.

Discrimination diagrams (TAS Total Alkalis vs Silica) indicate that the studied rock falls within the subalkaline field (Figure 6a), like other adakitic rocks and a silica-rich adakite reported by Martin et al. (2005). Additionally, the AFM (alkalis, iron, and magnesium) diagram demonstrates its calc-alkaline affinity. The An-Ab-Or normative diagram (Barker, 1979), which is ideal for silica rocks discrimination, shows that this rock falls in the tonalite field (not shown). In contrast, the An-Ab´-Or triangular diagram reveals a sodic character, except for the dacitic flow and the silica-rich adakite (Figure 6c).

According to the classification proposed by (Frost et al., 2001), the studied rock is slightly peraluminous, A/CNK [Al2O3/(CaO + Na_2O + K_2O)] >1 but <1.2, calcic and magnesian. Moreover, CIPW norm suggests that is a silica-oversaturated rock, with normative corundum (1.33%) and hypersthene (6.10%); see Table 3.

Zr/Y (7.9), Nb/Y (1.3), Ti/Zr (24.3), Ti/Y (192.9) and Ti/V (69.2) ratios suggest that this is a differentiated rock with cortical component (Pearce, 1982; McCulloch & Gamble, 1991) with low Nb (18 ppm), Y (14 ppm), Yb (0.88 ppm), and Sc (9 ppm) values. The last three trace element values fall among the typical ranges for adakites (Y<18 ppm, Yb<1.8 ppm, and Sc<10 ppm, (Defant & Drummond, 1990; Martin et al., 2005).

Even though in this study Sr values were not analyzed for rock discrimination purposes, in a LaN/YbN vs YbN diagram (Figure 6d), the studied rock, the dacitic flow, and he silica-rich adakite fall on the transition between normal arc rocks and the adakitic field. The La/Yb ratio is 24.98 and falls within the range of continental margin modern adakites (La/Yb<50; Sun et al., 2010) and close to silica-rich adakites (La/Yb~20; (Moyen., 2009). Furthermore, Sm/Yb=4.47 and La/Sm=5.60 ratios fall within the adakitic range (Sm/Yb=3-7 and La/Sm=~2-10; Dimalanta & Yumul Jr., 2008).

Alternatively, La/Nb ratio of the El Torito dome is equal to 1.22, which is different to the MORB value (0.8; Sun and McDonough, 1989) but resembles to continental crust (1.2; Rudnick and Fountain, 1995). Zr/Sm=28.24 ratio is higher than lower continental crust (Zr/Sm=24.29; Rudnick and Gao, 2003) and closer to the Al rich tonalites value (Zr/Sm> 25; Drummond et al., 1996), due to melting of an amphibolitic source.

The value of Cu (69 ppm) is higher than the corresponding value of the primitive mantle (30 ppm; Sun and McDonough, 1989) and the continental crust (27 ppm; Rudnick and Gao, 2003), but it falls within the MORB type oceanic crust range (60-120 ppm; Sun et al., 2011).

In this rock, the contents of Cr=87 ppm, Zr=111 ppm and Ce=48.73 ppm are closer to the mid-continental crust (Cr=83 ppm, Zr=125 ppm, Ce=45 ppm), while the Sm/Nd=0.20 ratio falls between the value for mid-continental crust (Sm/Nd=0.18) and the lower continental crust, (Sm/Nd=0.25; Rudnick and Fountain, 1995). LREE values (La, Ce, Nd, Sm, and Gd) are closer to the total of the continental crust (21.99 ppm vs 20 ppm, 43 ppm vs 43.73 ppm, 20 ppm vs 19.81 ppm, 3.9 ppm vs 3.93 ppm, and 3.7 ppm vs 3.83 ppm, respectively; Rudnick and Gao, 2014). The Gd/Yb ratio of the dome is 4.35 and greater than 1, which suggests the presence of a source involving garnet, and it is a value close to the typical adakites (3.4±1.1; Qing and Jörg, 2013). The Yb/Lu ratio of 6.7 is lower than HSA (~10; Moyen, 2009).

The rare earth spectrum normalized with respect to chondrites (Figure 7a) shows an enrichment of LREE with respect to HREE, which is typical of lavas formed under a subduction context, with values of $(La/Yb)_N$=17.91 (normalization values with respect to chondrites; Sun and Donough, 1989). Comparatively, the rare earth spectrum of the El Torito dome is quasiparallel to that of the remaining rocks; however, the $(La/Yb)_N$ ratio is enriched relative to that of the El Ventoso dome and San Cristóbal andesite $(La/Yb)_N$ ~12; Figure 7a

Additionally, despite some trace element values being absent from certain samples in this comparison, we included a normalization diagram relative to the primitive mantle (normalized values from Sun and McDonough, 1989), in which LILE and HFSE values are plotted. Two key observations emerge: 1) the enrichment of lithophile elements, and 2) the depletion of high field strength elements with strong ionic charges, which exhibit significant negative anomalies of Nb, P, Zr, Ti, and Yb. This pattern may be associated with the fractionation of amphibole, apatite, zircon, titanite, and titanomagnetite (Pearce, 1982). Furthermore, the negative anomalies of Nb, Zr, and Ti are characteristic of magmatism associated with subduction processes (Pearce, 1996).

Eu/Eu* (EuN/SmN+GdN) and Ce/Ce* (CeN/((LaN-PrN)/2) + PrN)) anomalies are negative, 0.66 and 0.55, respectively. The negative Eu anomaly is related to the fractionation of plagioclase in the magma consequently, it is situated closer to the upper crust (0.72; Rudnick and Gao, 2003), while the Ce negative anomaly is typical of volcanic arc rocks (Ce/Ce*<1; Hastie et al., 2013), suggesting the presence of subducted sediments involved in its genesis. This is also supported by the Th/Yb>2=3.41 ratio.

The glass contents in the dacite groundmass have rhyolitic composition (70%≤SiO_2≤79.42%) normal for andesites and porphyritic dacites with vitreous groundmass (Annen et al., 2006). Glass in this rock presents low TiO2 (<0.65%), FeO (<2%) and MnO, moderate MgO (0%≤MgO≤1.74%), (0.58%≤CaO≤2.93%), and high Na_2O (3.09%≤Na_2O≤5.19%) and Al_2O_3 (11.61%≤Al_2O_3≤16.22%) values (see Table 4). Regarding potassium contents, this glass is medium-to-potassium rich (1.43%≤K_2O≤6.85%), with ASI 0.92-1.09, meta-aluminous to slightly peraluminous, with quartz, albite, anorthite, orthoclase and corundum between 0-1.46% in the CIPW norm. On the An-Ab-Or triangular diagram (not shown), this glass falls in the granite and trondhjemite field. In general, the values of FeO/(FeO+MgO) ratio suggest a magnesian character, varying from calcic to calc-alkaline, according to the classification proposed by Frost et al. (2001). For comparison purposes, the composition of the interstitial glass in adakites from Baja California is rhyolitic (SiO_2=70,2-75,9%) with low TiO_2 (0,2-0,7%) values and intermediate Al_2O_3 (between 12,1 - 16,4%). Their analyses placed them in the field of tonalites, granodiorite, trondhjemite, and granite on a An-Ab-Or triangular diagram (Ribeiro, 2007).

.

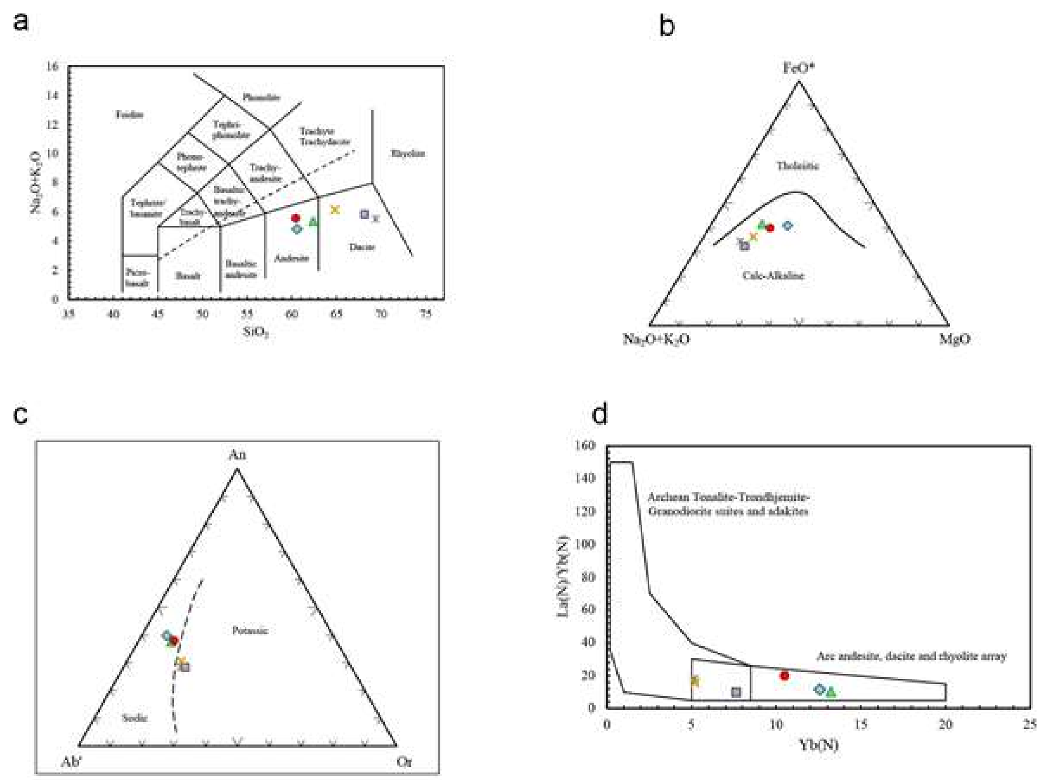

Figure 6. Classification of El Torito dome (gray cross) and compared rocks: El Ventoso dome (green triangle); dacitic-adakitic dome (gray square); Apan andesite (red circle); San Cristobal andesite (blue diamond); and silica-rich adakite (yellow cross; Martin et al., 2005). a – Na2O+K2O vs SiO2 classification diagram (TAS). b – AFM diagram, showing the calc-alkaline signature of the studied and compared rocks. c – An-Ab'-Or triangular diagram showing the sodic nature of El Torito, Apan andesite, and San Cristobal andesite; and d – (La/Yb)N vs YbN diagram (Defant and Drummond, 1990) showing their transitional character between normal arc rocks and the adakitic field. The silica-rich adakite and dacitic flow resemble the studied sample and fall within the adakite transitional field, while the remaining rocks are categorized in the normal arc field.

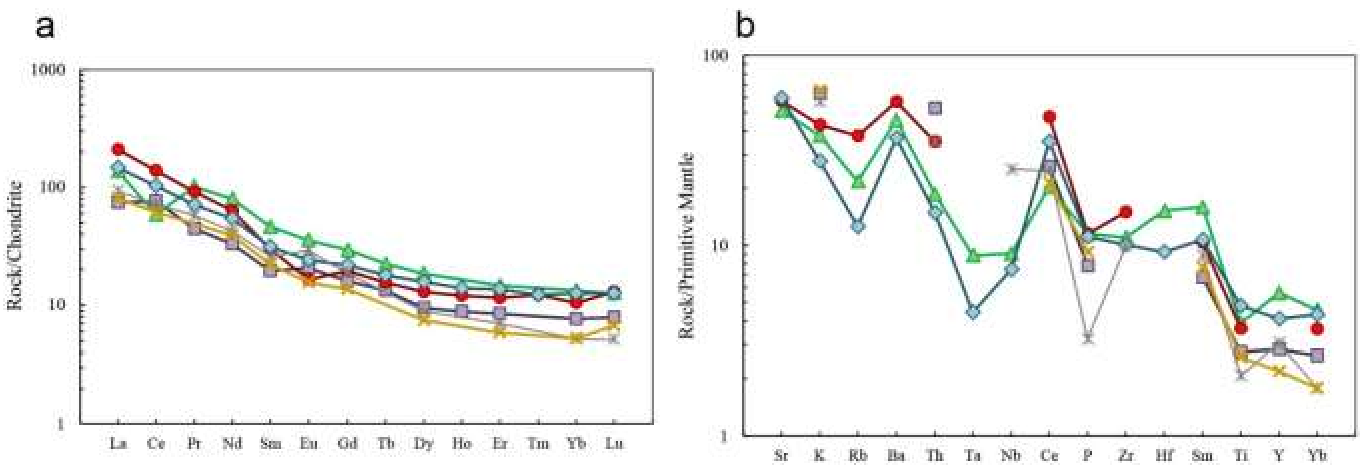

Figure 7. a – Normalization diagram with respect to chondrites (Sun and McDonough, 1989) showing LRE enrichment. b – Normalization diagram with respect to primitive mantle (Sun and McDonough, 1989) showing Nb, P, Ti, Zr and Yb negative anomalies, associated with the fractionation of amphibole, apatite, zircon, titanite and titanomagnetite. Symbology: studied rock, El Torito dome, gray cross. Rocks for comparison purposes: El Ventoso dome, green triangle; dacitic-adakitic dome, gray square; Apan andesite, red circle; San Cristobal andesite. blue diamond.

Table 4. Glass composition content in the dacite groundmass.[1]

	1	2	3	4	5	6	7	8	9
SiO_2	72.54	78.48	74.82	78.07	70.50	75.71	73.68	79.42	70.05
TiO_2	0.14	0.64	0.01	0.05	0.08	0.07	0.07	0.05	0.05
Al_2O_3	13.47	11.61	14.94	11.94	16.96	14.10	16.22	12.27	15.85
FeO	2.00	1.14	0.33	0.13	0.81	0.09	0.13	0.19	0.20
MnO	0.00	0.00	0.00	0.00	0.00	0.01	0.08	0.01	0.07
MgO	1.72	1.19	0.34	0.09	1.74	0.00	0.00	0.15	0.45
CaO	0.58	0.99	2.11	1.22	2.93	1.80	3.28	2.31	1.04
Na_2O	3.66	3.09	5.18	3.99	5.14	4.96	5.19	4.40	4.76
K2O	5.92	3.44	2.50	3.79	1.59	2.94	1.70	1.43	6.85
P_2O_5	0.30	0.05	0.00	0.10	0.00	0.00	0.01	0.00	0.31
Total	100.33	100.63	100.23	99.35	99.75	99.68	100.36	100.23	99.63

[1]Electron microprobe results.

4.3 Magma Physical-chemistry Parameters

Several authors confirm that aluminum contents in amphibole depends on crystallization pressure, and it can be used as a geobarometer. Hammarstron and Zen (1986) proposed a geobarometer based on aluminum in amphibole applied to plutonic rocks with typical calc-alkaline mineralogy. Hollister et al. (1987) proved its effectiveness in plutonic rocks and suggested that the pressure sensitive substitution in the amphibole is the tschermakitic component ($Ca_2(Mg_3Al_2)$ (Si_6Al_2) $O_{22}(OH)_2$); this is because high pressure favors alumina minerals in octahedral coordination rather than tetrahedral. Later, Johnson and Rutherford (1989) extended the use of this geobarometer to volcanic caldera rocks in California Valley, and Scmidt (1992) used it in tonalitic rocks.

Geobarometry based on aluminum contents in amphibole, as dependent on crystallization pressure, yielded crystallization conditions of ferromagnesian minerals as 5-5.8 kbar (±3 kbar; Hammarstrom and Zen, 1986), 5.2-6.2 kbar (±1 kbar; Hollister et al., 1987), 4.0-4.7 kbar (±0.5 kbar; Johnson and Rutherford, 1989) 5.4-6.2 kbar (±0.6 kbar; Schmidt, 1992) (Table 2). Therefore, mean crystallization pressure of amphiboles ranges between 4.38 and 5.8 kbars. Additionally, the geobarometer proposed by Johnson and Rutherford (1989), which has been applied to volcanic rocks with amphibole contents in equilibria with volcanic glass, yields minor uncertainty. Furthermore, 4.0-4.7 kbar (±0.5 kbar) correspond to an intermediate crustal depth, varying from 14.8 to 17.4 km, considering that 1 kb = 3.7 km. These results match with the formation depth of a cropping out, Na_2O enriched dioritic intrusive in the same caldera which crystallized between 3.3-3.8 kbars, and at a temperature range between 900-800 °C (Ortiz-Hernández and Escamilla-Casas, 2021).

Crystallization temperatures were determined by means of whole rock analysis and mineralogical data. According to CIPW norm data (Hollocher, 2004) the resulting liquidus temperature yielded 856 °C, while the geothermometer proposed by Jung and Pfänder (2007), which considers the Al_2O_3/TiO_2 ratio, yielded 904 ºC. Alternatively, apatite saturation suggests a temperature close to 800 °C (Green and Watson, 1982).

On the other hand, mineralogical data allowed us to determine crystallization pressure and temperature of the studied dome. Hence, the geothermometer proposed by Otten (1984) which considers titanium contents in amphibole, yielded crystallization temperatures between 808-850 ° C; while the semiquantitative geothermometer proposed by Ernst and Liu (1998) which considers titanium and aluminum contents in amphibole, provided a temperature range between 850-900 ° C. Furthermore, the geothermometer proposed by Holland and Blundy (1994) which considers the couple amphibole-plagioclase, yielded an average temperature of 805 °C. The geothermometer proposed by Putirka (2016) that considers the equilibrium between amphibole and magmatic liquid (equation 5), yielded a temperature range between 889-934 °C averaging 921 °C (±30 °C).

Alternatively, using the geothermometer titaniQ (Wark and Watson, 2006) TiO_2 analysis yielded 0.069 wt % contents in a quartz crystal, corroborating the crystallization temperature of this mineral (953 °C), which agrees with the temperatures from other geothermometers.

The presence of amphibole in dacite strongly suggests the hydrous character of the magma because amphibole stabilizes as a liquid phase with higher water contents (>3 wt%) especially in sodic melts (Sisson and Grove, 1993). Water content in the dacitic magma was obtained according to the hygrometer using the exchange reaction between plagioclase-magmatic liquid (Lange et al., 2009) yielding 3.9 to 4.7 wt % water, while applying equation 25b (Putirka, 2008) results in values between 3.7 - 5.9 wt % water. Oxygen fugacity in magma is high, between 10-12.23 - 10-11.30 bars according to data derived from amphibole (Putirka, 2016) which falls within the reported range for lavas with intermediate to acid composition (fO_2= 10-9.5 to 10-15.5; Carmichael, 1991).

Thermobarometric estimates derived from mineral-melt equilibrium calculations, combined with constraints on pre-eruptive H_2O*liq* contents, provide robust insights into the architecture of the magmatic plumbing system. The calculated pressures (~4.0–4.7 kbar), temperatures (~800-950 °C), and corresponding storage depths (~ 14.8-17.4 km) are consistent with magma storage within the intermediate crust. Raher than supporting the presence of a single, large, long-lived magma chamber, these conditions indicate a vertically extensive, trans-crustal system composed of multiple, interconnected magma storage and transport levels. Such a configuration implies distributed magma accumulation and episodic vertical transfer through the crust prior to eruption, in agreement with the inferred thermal and barometric gradients.

5. DISCUSSION

Although Sr is a key element commonly used in the discrimination of adakitic magmas, it is not available in the dataset presented here; therefore, the adakitic classification of the El Torito dome is necessarily constrained. However, adakitic affinity does not rely on a single elemental proxy but on a coherent geochemical signature reflecting magma generation in the presence of residual garnet and/or amphibole. In this regard, the rare earth element systematics provide a robust alternative discriminant. The El Torito sample displays strong LREE–HREE fractionation (La/Yb = 24.98), a feature widely interpreted as diagnostic of melts derived from garnet- and/or amphibole-bearing residues in subduction-related magmatic arcs (e.g., He et al., 2021; Rezaei-Kahkhei et al., 2022).

This interpretation is further supported by a suite of major- and trace-element characteristics consistent with adakitic compositions (SiO_2 >56%, Al_2O_3 >15%, MgO< 3%, TiO_2< 0.9% but more commonly < 0.6%, Na_2O>3.5 %, Cr≥ 30 ppm, Y<18 ppm, Yb<1.8 ppm, and Sc<10 ppm, 50 > La/Yb ratio >20 (Martin et al., 2005; Defant and Drummond, 1990; Sun et al., 2011; Drummond et al., 1996) these values are expected if considering partial melting of the basaltic crust in the presence of garnet, which is supported by the ratios of Y/Yb >10 and Sc/Yb (10.2) and Dy/Yb (2.55) vs La/Yb (25), suggesting residual garnet and amphibole. Fractionation of garnet and amphibole from a hydrous basaltic magma can produce magmatic fluids with normative corundum (1.4-3.5%) and adakitic characteristics (Macpherson et al., 2006). Consequently, while the lack of Sr prevents a fully classical adakite classification, the available geochemical evidence strongly indicates an adakitic affinity and is sufficient to support the petrogenetic interpretation proposed in this study.

Additionally, peraluminous character of the rock might result from the assimilation of continental crust or by the addition of sediments into the system. The petrogenetic conclusion for this rock is that it may have been produced by the melting of a basaltic slab associated with sediments in a hot subduction zone (subduction of young oceanic crust).

In Hidalgo state, the adakitic character of rocks has been recognized in several Miocenic volcanic sequences, e.g. Apan andesite (13.4±0.6 Ma; K/Ar), in the Apan volcanic field (García-Palomo et al., 2002; García-Palomo et al., 2018); in the Chichicuautla andesite (9.82±0.21 Ma; K/Ar) from the Chichicuautla-Tecocomulco volcanic field (Juárez-López, 2015); in the Jalapillas-Tecoaco dacitic domes, and El Chabacano dacitic breccia from the Epazoyucan-Singuilucan volcanic field (Aparicio-Canales and Contreras-Cruz, 2016) which can be correlated with the volcanic units of Santa Gertrudis and Zumate formations (23.7-21.6 Ma; K/Ar; Geyne et al., 1990).

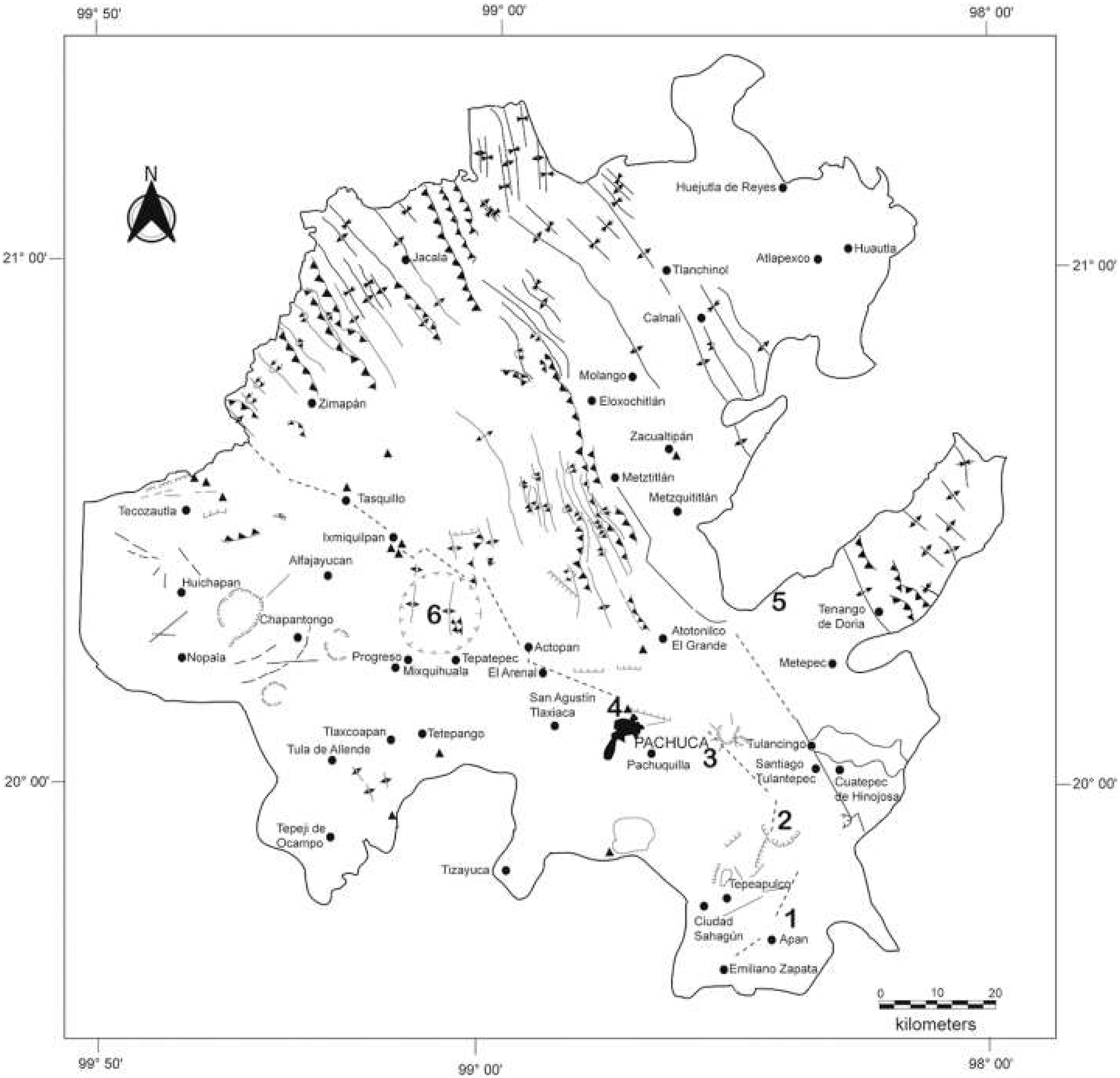

Figure 8. Simplified structural map of Hidalgo showing volcanic fields and sequences where the occurrence of adakitic rocks has been reported. 1 – Apan volcanic field, 2 – Chichicuautla-Tecocomulco volcanic field, 3 – Epazoyucan - Singuilucan volcanic field, 4 – Sierra de Pachuca, 5 – Tulancingo north region, 6 – Panales caldera, this study.

Finally, the adakitic character has also been found in the Pachuca-Real del Monte mining district (Martínez-González, 2018) and in dioritic to sienitic-dioritic intrusives in the northern region of Tulancingo (Sáenz-Pita, 2017; Figure 8).

Magmatism in the western sector of the state of Hidalgo has been dated radiometrically by (Kiyokawa, 1981and 1982) by conducting a K/Ar radiometric dating of an andesitic dome enriched in Na2O (3.85 wt%) in the locality of Benito Juárez south of Ixmiquilpan. This research yielded 27.2±1.4 Ma (Kiyokawa, 1982) while a hypabyssal rhyolite porphyry in El Cardonal county north of Ixmiquilpan, yielded a K/Ar 26.5±1.3 Ma radiometric age (Kiyokawa, 1982).Other rhyolites yielded ranges of

K/Ar ages between 27.1±1.4 and 26.5±1.3 Ma (Kiyokawa, 1982) pointing to Oligocene magmatism. North of the Panales caldera, a K/Ar radiometric age from an augite-hypersthene-hornblende quartz-monzonite enriched in Na2O (4.76%), which intrudes the El Doctor formation, yielded 23.2±1.2 Ma, corresponding to Oligocene age (Kiyokawa, 1982). Furthermore, a dioritic intrusive belonging to the Panales caldera, presents characteristics of Na2O enrichment, a typical signature of adakitic rocks (Ortiz-Hernández and Escamilla-Casas, 2021).

Additionally, representative analysis of volcanic rocks (andesites, dacites and rhyolites) and plutonic rocks (diorites, tonalites and monzodiorites) from the Panales caldera (own data and Barrera-Guerrero, 2009) and from areas to the north of the study area (Kiyokawa, 1981and 1982) strongly suggest the existence of adakitic magmatism in this sector of the TMVB (Figure 9).

The adakitic-trending dacitic magma related to the El Torito dome was most likely emplaced at the center of the Panales caldera following a renewed magmatic episode. Thermobarometric constraints indicate that this hot, sodic magma (~950–800 °C) originated at intermediate crustal depths (14.8–17.4 km) and subsequently ascended to the surface, forming a resurgent dacitic dome. During ascent from the magma reservoir, fractional crystallization processes were enhanced, accompanied by an increase in oxygen fugacity and likely minor crustal contamination.

Although no direct radiometric age is available for the El Torito dome, its petrogenetic and structural characteristics are consistent with the regional magmatic evolution documented for the Panales caldera and adjacent volcanic units. In this context, the studied dome provides relevant evidence for Cenozoic adakitic volcanism in the eastern sector of the Trans-Mexican Volcanic Belt, in agreement with the broader framework of early Miocene magmatism. This period marks the onset of calc-alkaline volcanism in the TMVB, extending beyond the Oligocene volcanic events reported in previous regional studies (Avellán et al., 2019).

6. CONCLUSIONS

The El Torito resurgent dome is a small volcanic edifice (~0.5 km²) characterized by remarkable lithological and textural homogeneity at both outcrop and hand-sample scales. Field observations show no evidence of compositional banding, textural variability, multiple intrusive or eruptive phases, magma mingling, or significant post-emplacement alteration that could indicate internal geochemical heterogeneity. Petrographic observations from samples collected at different stratigraphic levels further support interpretation of the dome as a single, coherent magmatic unit.

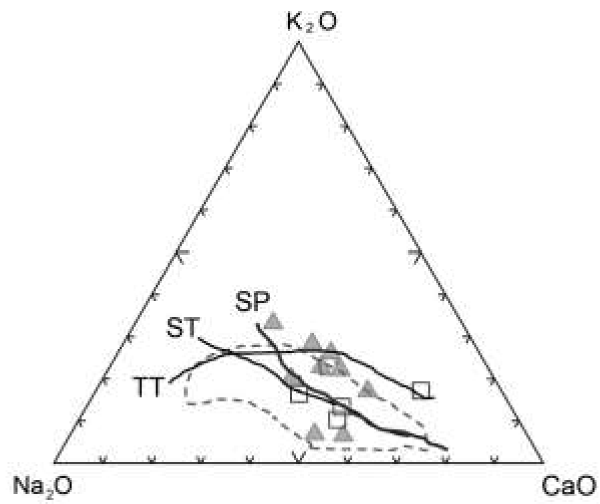

Figure 9. K2O-Na2O-CaO triangular diagram of representative rock analysis of the Panales caldera and nearby areas to the north, showing the trondhjemite (TT), sodic (ST), in comparison to the Sierra de Pachuca volcanic trends (SP). Discontinuous line represents the adakitic field. Squares represent volcanic rocks and solid triangles plutonic rocks

.

Whole-rock geochemical data obtained from a fresh, unaltered, and representative sample display internally consistent major- and trace-element abundances, low loss-on-ignition values, and element ratios indicative of a chemically uniform magma batch. These characteristics indicate that the analyzed sample reliably captures the primary magmatic signature of the dome and is representative of its bulk composition.

For volcanic bodies of comparable size and lithological uniformity, previous studies have shown that a single, carefully selected whole-rock analysis is sufficient to constrain bulk magma chemistry and to support first-order petrogenetic interpretations. In this context, additional geochemical sampling would be analytically redundant and unlikely to provide further constraints at the spatial and genetic scales addressed in this study. Accordingly, the sampling strategy adopted here is considered robust and appropriate for characterizing the magmatic processes responsible for the formation of the El Torito dome within the Panales Caldera.

Thermobarometric calculations based on mineral–melt equilibrium filters and pre-eruptive H_2Oliq contents further constrain the configuration of the magmatic plumbing system. The results indicate a vertically extensive crustal system composed of multiple interconnected magma transport and storage levels, rather than a single, voluminous magma chamber. These conditions suggest magma storage at intermediate crustal depths (~14.8–17.4 km; ~4.0–4.7 kbar) and temperatures ranging from ~800 to ~950 °C.

Although no direct radiometric age is currently available for the El Torito dome, its petrogenetic characteristics and structural setting are consistent with the regional magmatic evolution documented for the eastern sector of the Trans-Mexican Volcanic Belt, particularly within the framework of early Miocene calc-alkaline volcanism. Future geochronological work focused on identifying suitable datable mineral phases within the dome, or on refining indirect temporal constraints through adjacent volcanic units, will be essential to further constrain the timing of dome emplacement.

The petrographic and geochemical characteristics of the El Torito dome are consistent with previously reported adakitic magmatism in the eastern sector of the Trans-Mexican Volcanic Belt, particularly in the state of Hidalgo (e.g., Lucci et al., 2020). Together with other adakitic outcrops documented along the Sierra de Pachuca and the transitional zone between the Trans-Mexican Volcanic Belt and the Mexican Fold-and-Thrust Belt north of Tulancingo, the El Torito dome provides important constraints on the nature and evolution of magmatism in this sector of central Mexico. Furthermore, the present results highlight the role of transcrustal magmatic processes in the development of resurgent domes.

DECLARATION OF CONFLICT OF INTEREST

The authors declare no conflicts of interest

ACKNOWLEDGMENTS

The authors sincerely thank the reviewers of this contribution for their critical and enlightening recommendations.

7. REFERENCES

Acocella, V. (2007). Understanding caldera structure and development: An overview of analogue models compared to natural calderas. *Earth-Science Reviews*, 85(3–4), 125–160. https://doi.org/10.1016/j.earscirev.2007.08.004

Aguirre-Díaz, G. J. (1996). Volcanic stratigraphy of the Amealco caldera and vicinity, central Mexican Volcanic Belt. *Revista Mexicana de Ciencias Geológicas*; Vol 13 No 1, 1996; 10-51. Retrieved from https://repositorio.unam.mx/contenidos/4121481

Aguirre-Díaz, G. J. (2019). Volcanic stratigraphy of the Amealco caldera and vicinity, central Mexican Volcanic Belt. *Revista Mexicana De Ciencias Geológicas*, *13*(1), 10–51. Retrieved from https://rmcg.geociencias.unam.mx/index.php/rmcg/article/view/1135

Aguirre-Díaz, G.J., Nelson, S.A., Ferrari, L., López-Martínez, M. (1997). Ignimbrites of the central Mexican Volcanic Belt, Amealco and Huichapan calderas (Querétaro- Hidalgo). In: Aguirre-Díaz, G.J., Aranda-Gómez, J.J., Carrasco-Núñez, G., Ferrari, L. (Eds.), Magmatism and Tectonics of central and northwestern México—A selection of the 1997 IAVCEI General Assembly excursions, vol. 1. UNAM, Instituto de Geología, Excursión, México, D.F., pp. 1–39.

Aguirre-Díaz, G. J., & McDowell, F. W. (2000). Volcanic evolution of the Amealco caldera, central Mexico. In *Geological Society of America eBooks*. https://doi.org/10.1130/0-8137-2334-5.179

Anguita, F., Verma, S. P., Cacho, L. G., Milán, M., & Samaniego-M, D. (1991). Mazahua: una nueva caldera en el Cinturón Volcánico Mexicano. *Geofísica Internacional*, 30(3), 135–148. https://doi.org/10.22201/igeof.00167169p.1991.30.3.596

Anguita, F., Verma, S. P., Márquez, A., Vasconcelos-F, M., López, I., & Laurrieta, A. (2001). Circular features in the Trans-Mexican Volcanic Belt. *Journal of Volcanology and Geothermal Research*, 107(4), 265–274. https://doi.org/10.1016/s0377-0273(00)00297-3

Annen, C., Blundy, J. D., & Sparks, R. S. J. (2005). The genesis of intermediate and silicic magmas in deep crustal hot zones. *Journal of Petrology*, 47(3), 505-539. https://doi.org/10.1093/petrology/egi084

Aparicio-Canales, O., Contreras-Cruz, D. (2016). Caracterización petrográfica y geoquímica de las rocas volcánicas del área de Epazoyucan-Singuilucan, estado de Hidalgo: Mexico, Autonomous University of the State of Hidalgo, senior thesis, 116 p.

Avellán, D. R., Macías, J. L., Layer, P. W., Cisneros, G., Sánchez-Núñez, J. M., Gómez-Vasconcelos, M. G., Pola, A., Sosa-Ceballos, G., García-Tenorio, F., Reyes-Agustín, G., Osorio-Ocampo, S., García-Sánchez, L., Mendiola I. F., Martí, J., López-Loera, H., Benowits, B. (2019). Geology of the late Pliocene – Pleistocene Acoculco caldera Complex, eastern Trans-Mexican Volcanic Belt (Mexico). *Journal of Maps* 15 (2), 8-18. https:doi.org/10.1080/17445647.2018.1531075

Barker, F. (1979). Trondhjemite: Definition, Environment and Hypotheses of Origin. In *Developments in petrology* (pp. 1–12). https://doi.org/10.1016/b978-0-444-41765-7.50006-x

Barrera-Guerrero, S. & Ortiz-Hernandez, L. E. (2007). Episodios volcánicos en la Caldera Tolteca, estados Hidalgo, Mexico y Queretaro, México. XIII Congreso Nacional de Geoquímica, Pachuca de Soto, Hidalgo, México, *Actas INAGEQ*, 13 (1), 18-21.

Barrera-Guerrero, S. (2009). Caracterización geológica de la estructura semicircular Panales, Ixmiquilpan, estado de Hidalgo, México: Mexico, Autonomous University of the State of Hidalgo, senior thesis, 191 p.

Campos-Enriquez, J., & Gardun˜o-Monroy, V. (1995). Los Azufres silicic center (Mexico): inference of caldera structural elements from gravity, aeromagnetic, and geoelectric data. *Journal of Volcanology and Geothermal Research*, *67*(1–3), 123–152. https://doi.org/10.1016/0377-0273(94)00094-w

Castro-García, A., Córdoba-Méndez, D. (1994). Estratigrafía del área volcánica de Tulancingo, Hidalgo, México. *Pancromo* 23, Universidad Autónoma del Estado de Hidalgo, 1, 1, 26-39.

Carmichael, I. S. E. (1991). The redox states of basic and silicic magmas: a reflection of their source regions? *Contributions to Mineralogy and Petrology*, 106(2), 129–141. https://doi.org/10.1007/bf00306429

Carrasco, V. B. (1971). Litofacies de la Formación El Abra en la plataforma de Actopan, Hidalgo., México: *Revista del Instituto Mexicano del Petróleo*, 3,1,5-28

Cole, J., Milner, D., & Spinks, K. (2004). Calderas and caldera structures: a review. *Earth-Science Reviews*, 69(1–2), 1–26. https://doi.org/10.1016/j.earscirev.2004.06.004

Coltorti, M., Bonadiman, C., Faccini, B., Grégoire, M., O'Reilly, S. Y., & Powell, W. (2007). Amphiboles from suprasubduction and intraplate lithospheric mantle. *Lithos*, 99(1–2), 8–84. https://doi.org/10.1016/j.lithos.2007.05.009

Consejo de Recursos Minerales, 1995, Carta geológico-minera Ixmiquilpan (F14-C79) escala 1: 50,000.

Davies, J. H., & von Blanckenburg, F. (1995). Slab breakoff: A model of lithosphere detachment and its test in the magmatism and deformation of collisional orogens. *Earth and Planetary Science Letters*, 129(1-4), 85–102. https://doi.org/10.1016/0012-821X(94)00237-S

Defant, M. J., & Drummond, M. S. (1990). Derivation of some modern arc magmas by melting of young subducted lithosphere. *Nature*, 347(6294), 662-665. https://doi.org/10.1038/347662a0

Demant, A. (2019). Las fases del vulcanismo en México; una síntesis en relación con la evolución geodinámica desde el Cretácico. *Revista Mexicana De Ciencias Geológicas*, (1), 70–83. Retrieved from https://rmcg.geociencias.unam.mx/index.php/rmcg/article/view/1484

Dimalanta, C. B., & Yumul, G. P., Jr. (2008). Crustal thickness and adakite occurrence in the Philippines: Is there a relationship? *Island Arc*, 17(4), 421–431. https://doi.org/10.1111/j.1440-1738.2008.00634.x

Drummond, M. S., Defant, M. J., & Kepezhinskas, P. K. (1996). Petrogenesis of slab-derived trondhjemite–tonalite-dacite/adakite magmas. In *Geological Society of America eBooks*. https://doi.org/10.1130/0-8137-2315-9.205

Elkins, L.T., Grove, T.L. (1990). Ternary feldspar experiment and thermodynamic models: *American Mineralogist*, 75, 544-559.

Ernst, W. G., & Liu, J. (1998). Experimental phase-equilibrium study of Al- and Ti-contents of calcic amphibole in MORB; a semiquantitative thermobarometer. *American. Mineralogist*, 83(9–10), 952–969. https://doi.org/10.2138/am-1998-9-1004

Esawi, E. (2004). AMPH-CLASS: An Excel spreadsheet for the classification and nomenclature of amphiboles based on the 1997 recommendations of the International Mineralogical Association. *Computers & Geosciences*, 30(7),753–760. https://doi.org/10.1016/j.cageo.2004.05.007

Ferrari, L., Orozco-Esquivel, T., Manea, V., & Manea, M. (2012). The dynamic history of the Trans-Mexican Volcanic Belt and the Mexico subduction zone. *Tectonophysics*, 522–523,122–149. https://doi.org/10.1016/j.tecto.2011.09.018

Ferriz, H., & Mahood, G. A. (1987). Strong compositional zonation in a silicic magmatic system: Los Humeros, Mexican Neovolcanic Belt. *Journal of Petrology*, *28*(1), 171–209. https://doi.org/10.1093/petrology/28.1.171

Frost, B. R., Barnes, C. G., Collins, W. J., Arculus, R. J., Ellis, D. J., & Frost, C. D. (2001). A geochemical classification for granitic rocks. *Journal of Petrology*, 42(11), 2033–2048. https://doi.org/10.1093/petrology/42.11.2033

Galetto, F., Acocella, V., & Caricchi, L. (2017). Caldera resurgence driven by magma viscosity contrasts. *Nature Communications*, *8*, 1750. https://doi.org/10.1038/s41467-017-01632

García-Palomo, A., Macías, J. L., Tolson, G., Valdez, G., Mora, J. C. (2002). Volcanic stratigraphy and geological evolution of the Apan region, east-central sector of the Trans-Mexican Volcanic Belt: *Geofísica Internacional*, 41, 2, 133-150. https://doi.org/10.22201/igeof.00167169p.2002.41.2.282

García-Palomo A., Macías J. L., Jiménez A., Tolson, G., Mena, M., Sánchez-Núñez, J. M., Arce J. L.; Layer, P. W., Santoyo, M. A., Lermo-Samaniego, J. (2018). NW-SE Pliocene-Quaternary extension in the Apan-Acoculco region, eastern Trans-Mexican Volcanic Belt: *Journal of Volcanology and Geothermal Research*, 349, 240-255. doi.org/10.1016/j.jvolgeores.2017.11.005

García-Tovar, G. P., Martínez-Serrano, R. G., Solé, J., Correa-Tello, J. C., Núñez-Castillo, E. Y., Guillou, H., & Monroy-Rodríguez, E. (2015). Geología, geocronología y geoquímica del vulcanismo Plio-Cuaternario del Campo Volcánico Apan-Tecocomulco, Faja Volcánica Trans-Mexicana. *Revista Mexicana De Ciencias Geológicas,* 32(1). Retrieved from https://rmcg.geociencias.unam.mx/index.php/rmcg/article/view/278

Geyer, A., & MartÃ, J. (2014). A short review of our current understanding of the development of ring faults during collapse caldera formation. *Frontiers in Earth Science*, *2*. https://doi.org/10.3389/feart.2014.00022

Geyne, A. R., Fries, C., Segerstrom, K., Black, R. F., Wilson, I. F., 1990, Geology and Mineral Deposits of the Pachuca-Real del Monte District, Hidalgo, México, in, Clark, K. F.; Thompson, T. B., (eds.), Mexican Silver Deposits: *Australia, Society of Economic Geologists Guidebook Series, Society of Economic Geologists*, 6, 241-258. https://doi.org/10.5382/GB.06

Gómez-Alvarez, F., Garduño-Monroy, V. H., Sosa-Ceballos, G., Jiménez-Haro, A., Liotta, D., Gaitan-Ramirez, M. F., Brogi, A., Israde-Alcántara, I., Najera-Blas, S. M., Wheeler, W., Forster, M., & Garcia-Hernández, O. H. (2021). New constraints on tectonism and magmatism from the eastern sector of the Trans-Mexican Volcanic Belt (Chignahuapan Horst, Puebla, México). Journal Of South American Earth Sciences, 112, 103468. https://doi.org/10.1016/j.jsames.2021.103468

Gómez-Tuena, A., LaGatta, A. B., Langmuir, C. H., Goldstein, S. L., Ortega-Gutiérrez, F., & Carrasco-Núñez, G. (2003). Temporal control of subduction magmatism in the eastern Trans-Mexican Volcanic Belt: Mantle sources, slab contributions, and crustal contamination. *Geosystems, Geochemistry, Geophysics*, 4(8), 8912. https://doi.org/10.1029/2003gc000524

Gómez-Tuena, A., Orozco-Esquivel, T., Ferrari, L. (2005). Igneous petrogenesis of the Trans Mexican Volcanic Belt: *Boletín de la Sociedad Geológica Mexicana*, LVII, 3, 227-283. doi.org/10.18268/bsgm2005v57n3a2.

Green, T. H., & Watson, E. B. (1982). Crystallization of apatite in natural magmas under high pressure, hydrous conditions, with particular reference to ?Orogenic? rock series. *Contributions to Mineralogy and Petrology*, 79(1), 96–105. https://doi.org/10.1007/bf00376966

Guivel, C., Morata, D., Pelleter, E., Espinoza, F., Maury, R. C., Lagabrielle, Y., et al. (2006). Miocene to Late Quaternary Patagonian basalts (46–47 s): Geochronometric and geochemical evidence for slab tearing due to active spreading ridge subduction. *Journal of Volcanology and Geothermal Research*, 149(3), 346–370. https://doi.org/10.1016/j.jvolgeores.2005.09.002

Hammarstron, J.M., Zen, E. (1986). Aluminium in hornblende: An empirical igneous geobarometer: *American Mineralogist*, 71, 1297-1313.

Hastie, A.R., Mitchell, S.F., Treloar, P.J., Kerr, A.C., Neill, I., Barfod, D.N. (2013). Geochemical components in a Cretaceous Island arc: the Th/La–(Ce/Ce∗)Nd diagram and implications for subduction initiation in the inter-American region: *Litho*s,162–163, 57-69. doi:10.1016/j.lithos.2012.12.001

He, P., Huang, X., Yang, F., Wang, X. (2021). Mineralogy Constraints on Magmatic Processes Controlling Adakitic Features of Early Permian High-magnesium Diorites in the Western Tianshan Orogenic Belt. *Journal of Petrology,* 61, 11-12, 1-33. https://doi.org/10.1093/petrology/egaa114

Holland, T., & Blundy, J. (1994). Non-ideal interactions in calcic amphiboles and their bearing on amphibole-plagioclase thermometry. *Contributions to Mineralogy and Petrology*, 116(4), 433-447. https://doi.org/10.1007/bf00310910

Hollister, L. S., Grissom, G. C., Peters, E. K., Stowell, H. H., & Sisson, V. B. (1987). Confirmation of the empirical correlation of Al in hornblende with pressure of solidification of calc-alkaline plutons. *American Mineralogist*, 72, 231–239. https://ammin.geoscienceworld.org/content/72/3-4/231

Hollocher, K., 2004, CIPW Norm Calculation Program. Geology Department, Union College.

Johnson M.C & Rutherford, M.J. (1989). Experimental calibration of the aluminum-in-hornblende geobarometer with application to Long Valley caldera (California) volcanic rocks. *Geology*, 17(9), 837-841. https://doi.org/10.1130/0091-7613(1989)017%3C0837:ECOTAI%3E2.3.CO;2

Jung, S., Pfänder, J.A. (2007). Source composition and melting temperatures of orogenic granitoids-constraints from CaO/Na2O, Al2O3/TiO2 and accessory mineral saturation thermometry: *European Journal of Mineralogy*, 19, 6, 859-870. https://doi.org /10.1127/0935-1221/2007/0019-1774

Juárez-López, K., 2015, Evidencias de procesos magmáticos: Caracterización geoquímica e isotópica (Sr, Nd, Pb) del Campo Volcánico Chichicuautla-Tecocomulco, Estado de Hidalgo. México, Universidad Nacional Autónoma de México, Master's Thesis, 141 p.

Kiyokawa, M., 1981, Report on geological survey of the Pachuca-Zimapán area, central Mexico; phase II: México, Consejo de Recursos Minerales México, Metal Mining Agency of Japan & Japan International Cooperation Agency.195

Kiyokawa, M., 1982, Report on geological survey of the Pachuca-Zimapán area, central Mexico; phase III: Mexico, Consejo de Recursos Minerales México, Metal Mining Agency of Japan & Japan International Cooperation Agency. 121.

Lange, R. A., Frey, H. M., & Hector, J. (2009). A thermodynamic model for the plagioclase-liquid hygrometer/thermometer. *American Mineralogist*, 94(4), 494–506. https://doi.org/10.2138/am.2009.3011

Leake, B. E., Woolley, A. R., Arps, C. E. S., Birch, W. D., Gilbert, M. C., Grice, J. D., Hawthorne, F. C., Kato, A., Kisch, H. J., Krivovichev, V. G., Linthout, K., Laird, J., Mandarino, J., Maresch, W. V., Nickel, E. H., Rock, N. M. S., Schumacher, J. C., Smith, D. C., Stephenson, N. C. N., . . . Youzhi, G. (1997). Nomenclature of amphiboles; Report of the Subcommittee on Amphiboles of the International Mineralogical Association Commission on New Minerals and Mineral Names. *Mineralogical Magazine*, *61*(405), 295–310. https://doi.org/10.1180/minmag.1997.061.405.13

Lipman, P. W. (1997). Subsidence of ash-flow calderas: relation to caldera size and magma-chamber geometry. *Bulletin of Volcanology*, *59*(3), 198–218. https://doi.org/10.1007/s004450050186

Lipman, P. W., Zimmerer, M. J., & McIntosh, W. C. (2015). An ignimbrite caldera from the bottom up: Exhumed floor and fill of the resurgent Bonanza caldera, Southern Rocky Mountain volcanic field, Colorado. *Geosphere*, *11*, 1902–1947.

Liu, M., & Gao, H. (2023). Role of subduction dynamics on the unevenly distributed volcanism at the Middle American subduction system. Scientific Reports, 13(1), 14697. https://doi.org/10.1038/s41598-023-41740-y

López-Hernández, A., García-Estrada, G., Aguirre-Díaz, G., González-Partida, E., Palma-Guzmán, H., & Quijano-León, J. L. (2009). Hydrothermal activity in the Tulancingo–Acoculco Caldera Complex, central Mexico: *Exploratory studies. Geothermics*, *38*(3), 279–293. https://doi.org/10.1016/j.geothermics.2009.05.001

Lucci, F., Carrasco-Núñez, G., Rossetti, F., Theye, T., White, J. C., Urbani, S., Azizi, H., Asahara, Y., & Giordano, G. (2020). Anatomy of the magmatic plumbing system of Los Humeros Caldera (Mexico): implications for geothermal systems. *Solid Earth*, 11(1), 125. https://doi.org/10.5194/se-11-125-2020

Luo, C., Wang, R., Nebel, O., & Li, Q. (2024). Amphibole fractionation as a key driver for oxidation of magmas in convergent margins. *Earth and Planetary Science Letters*, *641*, 118851. https://doi.org/10.1016/j.epsl.2024.118851

Macpherson, C. G., Dreher, S. T., & Thirlwall, M. F. (2006). Adakites without slab melting: High pressure differentiation of island arc magma, Mindanao, the Philippines. *Earth and Planetary Science Letters*, *243*(3–4), 581–593. https://doi.org/10.1016/j.epsl.2005.12.034

Mahood, G. A. (1980). Geological evolution of a pleistocene rhyolitic center — Sierra La Primavera, Jalisco, México. *Journal of Volcanology and Geothermal Research*, *8*(2–4), 199–230. https://doi.org/10.1016/0377-0273(80)90105-5

Maldonado-Sánchez, G., & Schaaf, P. (2005). Geochemical and isotope data from the Acatlán Volcanic Field, western Trans-Mexican Volcanic Belt: Origin and evolution. *Lithos,* 82(3-4), 455-470. https://doi.org/10.1016/j.lithos.2004.09.030

Martínez-González, I.R., 2018, Aportaciones petrográficas, geoquímicas e isotópicas, en la caracterización petrogenética de rocas volcánicas de la sierra de Pachuca. Mexico, Universidad Nacional Autónoma de Mexico, Facultad de Ciencias, Senior thesis, 120 p.

Márquez, A., Oyarzun, R., Doblas, M., Verma, S. P. (1999). Alkalic (ocean-island basalt type) and calc-alkalic volcanism in the Mexican volcanic belt; a case for plume-related magmatism and propagating rifting at an active margin? Geology, 27(1), 51-54. https://doi.org/10.1130/0091-7613(1999)027<0051:AOIBTA>2.3.CO;2

McCulloch, M., Gamble, J. (1991). Geochemical and geodynamical constraints on subduction zone magmatism. *Earth and Planetary Science Letters*, *102*(3–4), 358–374. https://doi.org/10.1016/0012-821x(91)90029-h

Martin, H., Smithies, R., Rapp, R., Moyen, J., & Champion, D. (2005). An overview of adakite, tonalite–trondhjemite–granodiorite (TTG), and sanukitoid: relationships and some implications for crustal evolution. *Lithos*, *79*(1–2), 1–24. https://doi.org/10.1016/j.lithos.2004.04.048

Milán, M., Yañez, C., Navarro L., I., & Verma, S. P. (1993). Geología y geoquímica de elementos mayores de la Caldera de Huichapan, Hidalgo, México. *Geofísica Internacional*, *32*(2), 261–276. https://doi.org/10.22201/igeof.00167169p.1993.32.2.560

Mooser, F. (1972). The Mexican Volcanic Belt structure and tectonics. *Geofísica Internacional*, *12*(2),55–70. https://doi.org/10.22201/igeof.00167169p.1972.12.2.1024

Moyen, J. (2009). High Sr/Y and La/Yb ratios: The meaning of the "adakitic signature." Lithos, *112*(3–4), 556–574. https://doi.org/10.1016/j.lithos.2009.04.001

Negendank, J. F. W., Emmermann, R., Krawczyk, R., Mooser, F., Tobschall, H., & Werle, D. J. (1985). Geological and geochemical investigations on the eastern Trans-Mexican Volcanic Belt. *Geofísica Internacional*, *24*(4), 477–575. https://doi.org/10.22201/igeof.00167169p.1985.24.4.2178

Ortiz-Hernández, L. E., Hernández-Avelino I. (2006). Caracterización de la caldera Mezquital, estado de Hidalgo. *V Reunión Nacional de Ciencias de la Tierra, resumen*. 15-17 septiembre 2006, Puebla, Pue.

Ortiz-Hernández, L. E. O. & Escamilla-Casas, J. C. (2021). Mineralogía y geoquímica de un intrusivo diorítico del centro de México. *Tópicos De Investigación En Ciencias De La Tierra Y Materiales*, 8(8), 47–53. https://doi.org/10.29057/aactm.v8i8.7505

Ortiz Hernández, L. E., & Escamilla Casas, J. C. (2024). Ruby Xenocrystals in Dacite from Central Mexico. *Geofísica Internacional*, 63(3), 977–988. https://doi.org/10.22201/igeof.2954436xe.2024.63.3.1727

Otten, M. T. (1984). The origin of brown hornblende in the Artfjället gabbro and dolerites. *Contributions to Mineralogy and Petrology*, 86(2), 189–199. https://doi.org/10.1007/bf00381846

Pasquare, G., Vezzoli, L., & Zanchi, A. (1987). Morphological and structural model of Mexican Volcanic Belt. *Geofísica Internacional*, 26(2), 159-175. https://doi.org/10.22201/igeof.00167169p.1987.26.2.1107

Pearce, J. A. (1982). Trace element characteristics of lavas from destructive plate boundaries. In *John Wiley and Sons eBooks* (pp. 525–548). http://orca.cf.ac.uk/8625/

Pearce, J.A. (1996). A User's Guide to Basalt Discrimination Diagrams. In: Wyman, D.A., Ed., *Trace Element Geochemistry of Volcanic Rocks: Applications for Massive Sulphide Exploration*, Geological Association of Canada, Short Course Notes, Vol. 12, 79-113.

Putirka, K. D. (2008). Thermometers and barometers for volcanic systems. *Reviews in Mineralogy and Geochemistry*, 69(1), 61–120. https://doi.org/10.2138/rmg.2008.69.3

Putirka, K. (2016). Amphibole thermometers and barometers for igneous systems and some implications for eruption mechanisms of felsic magmas at arc volcanoes. American Mineralogist, 101(4), 841–858. https://doi.org/10.2138/am-2016-5506

Qian, Q., & Hermann, J. (2013). Partial melting of lower crust at 10–15 kbar: constraints on adakite and TTG formation. *Contributions to Mineralogy and Petrology*, *165*(6), 1195–1224. https://doi.org/10.1007/s00410-013-0854-9

Ramírez-Ramírez, B. B., 2016, Campo volcánico San Vicente, estado de Hidalgo, Faja Volcánica Trans-mexicana: variaciones geoquímicas e isotópicas y su relación con el retroceso del arco hacia la trinchera: Mexico, Instituto Politécnico Nacional, ESIA-Unidad Ticomán, Master's thesis, 157 p.

Reyes-Moreno, J. R., Corona, F. P., Santillán, I. Á., & Hernández, L. O. (2019). Combinación de métodos potenciales y percepción remota para el análisis geológico-estructural de la caldera panales, Hidalgo, México. *Tópicos De Investigación en Ciencias de la Tierra y Materiales*, *6*(6), 123–129. https://doi.org/10.29057/aactm.v6i6.5021

Rezaei-Kahkhaei M., Corfu F., Galindo C., Rahbar R, Ghasemi H. (2022). Adakite genesis and plate convergent process: Constraints from whole rock and mineral chemistry, Sr, Nd, Pb isotopic compositions and U-Pb ages of the Lakhshak magmatic suite, East Iran. *Lithos* 426- 427 106806. https://doi.org/10.1016/j.lithos.2022.106806

Ribeiro, L. J., 2007, Magmas adakitiques: composition des amphiboles et contraintes géo barométriques. Université Bretagne Occidentale, Mémoire de stage de Master 2, Spécialité: Géochimie et pétrologie, 85 p.

Ribeiro, J. M., Maury, R. C., & Gr.goire, M. (2016). Are adakites slab melts or high-pressure fractionated mantle melts? *Journal of Petrology*, 57(5), 839–862. https://doi.org/10.1093/petrology/egw023

Rudnick, R. L., & Fountain, D. M. (1995). Nature and composition of the continental crust: A lower crustal perspective. *Reviews of Geophysics*, *33*(3), 267–309. https://doi.org/10.1029/95rg01302

Rudnick, R., & Gao, S. (2003). Composition of the continental crust. In *Elsevier eBooks* (pp. 1–64). https://doi.org/10.1016/b0-08-043751-6/03016-4

Schmidt, M. W. (1992). Amphibole composition in tonalite as a function of pressure: an experimental calibration of the Al-in-hornblende barometer. *Contributions to Mineralogy and Petrology*, *110*(2–3), 304–310. https://doi.org/10.1007/bf00310745

Saénz-Pita M. R, 2017, Geologic and Geochemical Studies of the North Region of Tulancingo, Hidalgo, Focused on Mining Prospection, Mexico, IPN-ESIA Unidad Ticomán, Master's thesis, 87 p.

Segerström, K. (1961). Geología del Suroeste del Estado de Hidalgo y del Noreste del Estado de México. *Boletín de la Asociación Mexicana de Geólogos Petroleros, 13* (3-4), 147-168.

Sheth, H. C., Torres-Alvarado, I. S., & Verma, S. P. (2000). Beyond Subduction and Plumes: A Unified Tectonic-Petrogenetic Model for the Mexican Volcanic Belt. *International Geology Review*, 42(12), 1116-1132. https://doi.org/10.1080/00206810009465129

Sheth, H. C., Torres-Alvarado, I. S., & Verma, S. P. (2002). What Is the «Calc-alkaline Rock Series»? *International Geology Review*, 44(8), 686-701. https://doi.org/10.2747/0020-6814.44.8.686

Sillis-Esquivel, J., 2011, Modelo análogo de tipo "caja de arena" aplicado a la estructura semicircular e Santa María Amajac, Edo. De Hidalgo, ION-ESIA Unidad Ticonán, Master's thesis, 152 p.

Sisson, T. W., & Grove, T. L. (1993). Experimental investigations of the role of H2O in calc-alkaline differentiation and subduction zone magmatism. *Contributions to Mineralogy and Petrology*, *113*(2), 143–166. https://doi.org/10.1007/bf00283225

Sun, S., & McDonough, W. F. (1989). Chemical and isotopic systematics of oceanic basalts: implications for mantle composition and processes. *Geological Society London Special Publications*, *42*(1), 313–345. https://doi.org/10.1144/gsl.sp.1989.042.01.19

Sun, W., Zhang, H., Ling, M. X., Ding, X., Chung, S. L., Zhou, J., … Fan, W. (2010). The genetic association of adakites and Cu–Au ore deposits. *International Geology Review*, *53*(5–6), 691–703. https://doi.org/10.1080/00206814.2010.507362

Sun, W., Ling, M., Chung, S., Ding, X., Yang, X., Liang, H., Fan, W., Goldfarb, R., & Yin, Q. (2011). Geochemical constraints on adakites of different origins and copper mineralization. *The Journal of Geology*, *120*(1), 105–120. https://doi.org/10.1086/662736

Velasco-Tapia, F., Verma, S.P. (2013). Magmatic processes at the volcanic front of Central Mexican Volcanic Belt: Sierra Chichinautzin Volcanic Field (Mexico). *Turkish Journal of Earth Sciences,* 22, 32–60. https://doi.org/10.3906/yer-1104-9

Verma, S.P., 2002. Absence of Cocos plate subduction-related mafic volcanism in southern Mexico: a unique case on Earth? *Geology,* 1,095–1,098. https://doi.org/ 10.1130/0091-7613(2002)030<1095:AOCPSR>2.0.CO;2

Wark, D. A., & Watson, E. B. (2006). TitaniQ: a titanium-in-quartz geothermometer. *Contributions to Mineralogy and Petrology*, *152*(6), 743–754. https://doi.org/10.1007/s00410-006-0132-1

Weber, G., Caricchi, L., & Arce, J. L. (2020). The Long-Term Life-Cycle of Nevado de Toluca Volcano (Mexico): Insights into the Origin of Petrologic Modes. *Frontiers in Earth Science*, 8. https://doi.org/10.3389/feart.2020.563303